ACS OMEGA

Open Access

http://pubs.acs.org/journal/acsodf

Article

Conformational Flexibility of D1-Glu189: A Crucial Determinant in Substrate Water Selection, Positioning, and Stabilization within the Oxygen-Evolving Complex of Photosystem II

Hiroshi Isobe,* Takayoshi Suzuki, Michihiro Suga, Jian-Ren Shen, and Kizashi Yamaguchi

Cite This: *ACS Omega* 2024, 9, 50041−50048

Read Online

ACCESS | Metrics & More | Article Recommendations | Supporting Information

ABSTRACT: Photosynthetic water oxidation is a vital process responsible for producing dioxygen and supplying the energy necessary to sustain life on Earth. This fundamental reaction is catalyzed by the oxygen-evolving complex (OEC) of photosystem II, which houses the Mn_4CaO_5 cluster as its catalytic core. In this study, we specifically focus on the D1-Glu189 amino acid residue, which serves as a direct ligand to the Mn_4CaO_5 cluster. Our primary goal is to explore, using density functional theory (DFT), how the conformational flexibility of the D1-Glu189 side chain influences crucial catalytic processes, particularly the selection, positioning, and stabilization of a substrate water molecule within the OEC. Our investigation is based on a hypothesis put forth by Li et al. (*Nature*, **2024**, *626*, 670), which suggests that during the transition from the S_2 to S_3 state, a specific water molecule temporarily coordinating with the Ca ion, referred to as O6*, may exist as a hydroxide ion (OH^-). Our results demonstrate a key mechanism by which the detachment of the D1-Glu189 carboxylate group from its coordination with the Ca ion allows the creation of a specialized microenvironment within the OEC that enables the selective attraction of O6* in its deprotonated form (OH^-) and stabilizes it at the catalytic metal (Mn_D) site. Our findings indicate that D1-Glu189 is not only a structural ligand for the Ca ion but may also play an active and dynamic role in the catalytic process, positioning O6* optimally for its subsequent participation in the oxidation sequence during the water-splitting cycle.

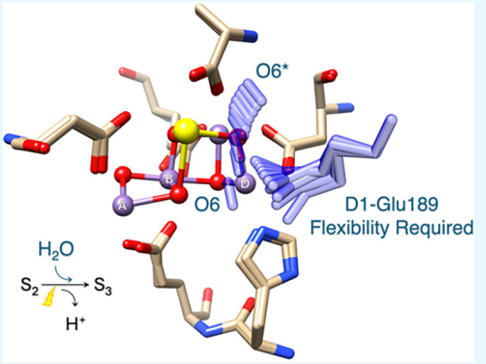

1. INTRODUCTION

Most life activities in nature rely on photosynthesis, a fundamental biological process that harnesses solar energy to convert carbon dioxide into organic compounds essential for living organisms.[1] Photosynthetic organisms such as cyanobacteria, algae, and higher plants have evolved remarkably sophisticated mechanisms to extract electrons from water, enabling their widespread distribution on Earth. Conversely, aerobic organisms have acquired the ability to use dioxygen, a byproduct of photosynthesis, through respiratory functions that resist the toxicity of oxygen and facilitate substantial energy transformations. This adaptation supports various metabolic processes that are essential for growth, development, and life maintenance, while also enabling the recycling of limited carbon between the inorganic environment and the biological realm using the boundless energy of sunlight, thereby sustaining the delicate balance of ecosystems. Given that photosynthesis is the only process in the biosphere capable of splitting water to produce dioxygen, deciphering its mechanism is of utmost importance, not only for its intrinsic scientific value but also for addressing environmental and energy challenges related to global warming and fossil fuel depletion.[2,3]

At the heart of the photosynthetic machinery is photosystem II (PSII), a multisubunit protein−cofactor complex located in the thylakoid membrane of chloroplasts and cyanobacterial cells. PSII plays a crucial role in supplying energized electrons necessary for the photosynthetic processes by splitting water molecules.[4−7] The initiation of PSII function begins with a light-induced charge separation between a specialized chlorophyll dimer (P680) and a pheophytin (Pheo) electron acceptor, forming a $P680^+Pheo^-$ radical pair. The electron that is transferred to $Pheo^-$ is then relayed through a series of redox reactions, moving first to a primary quinone electron acceptor and eventually to a secondary quinone electron acceptor on the stromal side of the thylakoid membrane. Simultaneously, the electron hole generated on $P680^+$ is passed to the catalytic core of the oxygen-evolving complex (OEC), comprised of an oxo-bridged heteronuclear Mn_4CaO_5 cluster, on the luminal side of the membrane via a redox-active tyrosine residue, D1-

Received: November 2, 2024
Revised: November 25, 2024
Accepted: November 28, 2024
Published: December 5, 2024

Tyr161 (Y_Z). This cluster serves as the catalytic center for water oxidation, a complex four-electron oxidation process that is facilitated by Y_Z. The Mn_4CaO_5 cluster undergoes a cycle of oxidation states, known as the S-state cycle, which consists of five distinct intermediates denoted as S_i states (i = 0−4). Each state represents a specific number of accumulated oxidizing equivalents or holes within the cluster, which are crucial for driving the water-splitting reaction.

Recent advancements made possible by serial femtosecond X-ray crystallography have provided unprecedented insights into the structural dynamics within PSII, particularly regarding the Mn cluster and its surrounding protein environment. These studies have offered high-resolution views of their structural evolution across key intermediates of the water-splitting cycle, namely the S_1, S_2, S_3, and S_0 states.[8−15] With high spatial and temporal resolution, this technique has shed light not only on the static structural features but also on the intricate interplay of protein dynamics that govern critical functional events, such as water ingress and binding, proton transfer, and dioxygen formation. This is especially evident in the S_2 to S_3 transition; over a slower time scale, extensive shifts in amino acid side chains and backbone configurations take place, while faster, more localized displacements of the Mn and Ca ions within the Mn_4CaO_5 cluster occur simultaneously. One of the most significant events during this transition is the binding and activation of a new water molecule, referred to as O6 or O_X, in the vicinity of the existing O5 oxygen atom within the Mn cluster. This event is a key step toward the formation of the O5−O6 bond, which is essential for the oxygen-evolving mechanism. The identity of O5 and O6 continues to be a subject of ongoing investigation. However, X-ray crystallography studies have measured O−O distances ranging from 1.9 to 2.2 Å,[9−11,15] suggesting that O5 and O6 might exist predominantly in an oxyl−oxo form poised for bond formation or as a mixture of oxyl−oxo and hydroxo−oxo forms.

The OEC exhibits remarkable structural and electronic flexibility, enabling it to accommodate sequential oxidation state changes while efficiently binding and chemically transforming substrate water molecules throughout the catalytic cycle. This flexibility is largely due to the well-coordinated environment that supports the catalytic activity of the Mn_4CaO_5 cluster, comprising six carboxylate ligands (D1-Asp170, D1-Glu189, D1-Glu333, D1-Asp342, D1-Ala344, and CP43-Glu354), along with a histidine residue (D1-His332), as illustrated in Figure 1.[16−18] Among these ligands, D1-Glu189 is particularly notable for its dynamic behavior during the S_2 to S_3 transition. In lower oxidation states, D1-Glu189 serves as a structural ligand by coordinating with both the Ca and Mn_D ions within the Mn_4CaO_5 cluster. However, upon the application of a second flash of light (2F) that advances the OEC to the S_3 state, D1-Glu189 undergoes a displacement of approximately 0.2 Å away from the Ca ion, which appears to be a critical adjustment that facilitates the catalytic progression.[8−12,14,15] A recent time-resolved crystallographic study conducted by Li et al. has further provided new insights into this transition. Their observations detected the emergence of new electron density, designated as O6*, within the coordination sphere of the Ca ion approximately 200 ns after 2F.[15] Notably, this newly identified electron density gradually diminishes after around 200 μs, a time frame that coincides with the appearance and stabilization of increased O6 electron density at the Mn_D site within the Mn_4CaO_5 cluster. These findings suggest that the initially coordinated O6* is likely a water-derived species that is subsequently repositioned from its temporary location near the Ca ion to the Mn_D site, where it becomes incorporated as a substrate water molecule essential for catalytic activity.

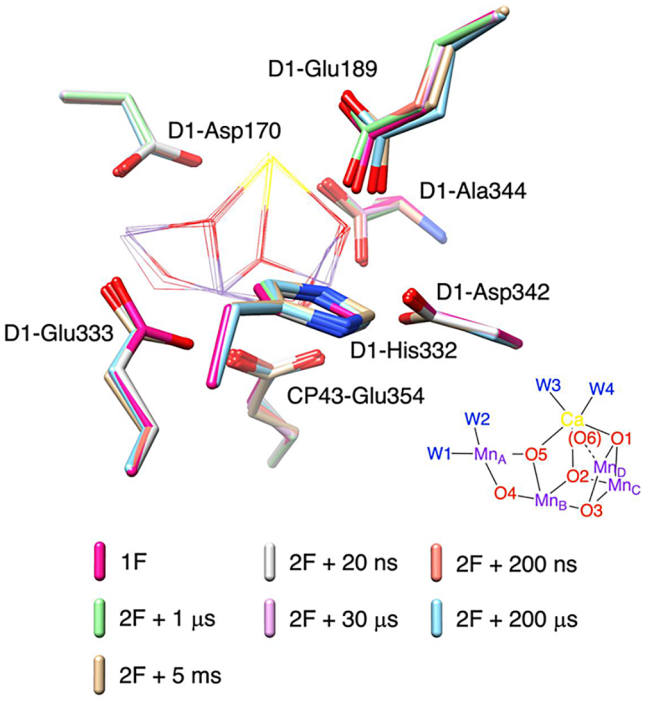

Figure 1. Conformational changes of amino acid residues within the primary coordination sphere of the Mn cluster observed experimentally during the S_2 to S_3 transition.[15] Structural models captured at 1F (red), and time points at 20 ns (gray), 200 ns (orange), 1 μs (light green), 30 μs (pink), 200 μs (cyan), and 5 ms (gold) after 2F are superimposed. The inorganic Mn_4CaO_5 cluster is displayed in wireframe, while seven amino acid residues in the primary coordination sphere are shown in stick representation.

Based on these findings, the present study focuses on the specific role of D1-Glu189 within the OEC. Assuming, as proposed by Li et al., that the transient O6*species could exist in the form of a hydroxide ion (OH^-),[15] we use density functional theory (DFT) calculations to investigate how the conformational flexibility of the D1-Glu189 side chain contributes to the selection, guidance, and binding of the transient O6* within the OEC. Through this analysis, we aim to demonstrate that D1-Glu189 goes beyond serving merely as a coordinating ligand for the Ca and Mn_D ions and plays an active and dynamic role in catalytic processes that have been challenging to directly capture using current XFEL-based experimental techniques.

2. COMPUTATIONAL DETAILS

We constructed an OEC model using the XFEL crystallographic model of PSII (PDB ID 6JLL, monomer A), as illustrated in Figure S1. This model includes a total of 407 atoms comprising the inorganic Mn_4CaO_5 cluster, four terminal aqua/hydroxo ligands coordinated to Ca and Mn_A, an additional O6* ligand near the Ca site, 15 crystallographic water molecules, a chloride ion (Cl^-), and the following amino acid residues: D1-Asp61, D1-Asn87, D1-Tyr161 (Tyr_Z), D1-Gln165, D1-Ser169, D1-Asp170, D1-Asn181, D1-Val185, D1-Phe182 (backbone only), D1-Glu189, D1-His190, D1-Asn298 (fragment), D2-Lys317 (fragment), D1-His332, D1-Glu333,

https://doi.org/10.1021/acsomega.4c09981
ACS Omega 2024, 9, 50041−50048

D1-Ala336, D1-His337, D1-Asp342, D1-Ala344 (C-terminus), CP43-Glu354, CP43-Arg357, D1-Asn296, CP43-Leu401, CP43-Val410, and CP43-Ala411. Four Mn ions in the Mn_4CaO_5 cluster are labeled as Mn_A, Mn_B, Mn_C and Mn_D, as shown in Figures 1 and S1, which correspond to Mn4A, Mn3B, Mn2C, and Mn1D in the crystallographic structures. The oxidation state of Mn_D is assigned as Mn^{III}, while Mn_A, Mn_B, and Mn_C are in the Mn^{IV} oxidation state. Geometry optimizations were performed with a spin multiplicity of 14 using the B3LYP functional[19−21] enhanced by the D3 version of Grimme's empirical dispersion correction and the Becke−Johnson (BJ) damping function,[22,23] as implemented in Gaussian 16.[24] The Los Alamos (LANL2DZ) pseudopotential basis set was used to represent Ca and Mn,[25−27] while all other atoms were described using the 6-31G(d) basis set. These basis sets are labeled as BS1. The impact of steric effects resulting from the protein fold was taken into account by constraining the atomic positions of the backbone and the entire residues of D1-Gln165, D1-Asn298, D2-Lys317, D1-Asn296, CP43-Leu401, CP43-Val410, CP43-Ala411, and D1-Asn296, CP43-Leu401, CP43-Val410, and CP43-Ala411 located at the periphery of the model to their X-ray structure coordinates during the optimization of geometry. Single-point energies were computed employing the nonstandard B3LYP* functional, with a 5% reduction in the percentage of the Hartree−Fock exchange from 20 to 15%,[28] in combination with the extended basis set comprising the Stuttgart/Dresden (SDD) pseudopotential basis set[29,30] for Ca and Mn, and 6-311G(d,p) for all other atoms, designated as BS2. For these single-point calculations, the model system was immersed in a solvent using the IEFPCM model[31] with a dielectric constant of 5.7 (corresponding to chlorobenzene) to approximate the low polarizability of the protein interior.

3. RESULTS AND DISCUSSION

Our study focuses on the role of the specific amino acid residue D1-Glu189 within the OEC. This residue is characterized by its relatively long side chain terminating in a carboxylate group, which allows it to influence the local protein environment by modulating the hydrogen-bond network and coordinating interactions. The main objectives of this research are to understand how the flexible nature of this long side chain manifests within the OEC and to evaluate its impact on the selective attraction, precise guidance, and effective stabilization of a substrate water molecule. A key hypothesis underlying this investigation is that during the S_2 to S_3 transition, a specific water molecule (O6*) may temporarily interact with a Ca ion in the form of a hydroxide ion (OH^-).[15] This transient association is assumed to be essential for its eventual incorporation into the Mn_4CaO_5 cluster, making it crucial to investigate its detailed mechanism.

The side chain of the glutamate residue is connected with the C_α atom of the backbone via two sp^3 hybridized carbon atoms (C_β and C_γ), enabling it to potentially orient in various directions, as depicted in Figure 2. The side chain orientation can be described with a set of three dihedral angles (D_1, D_2, D_3), with D_1 somewhat restricted due to steric interference between C_γ and the main chain. In the actual protein environment, the ranges of D_2 and D_3 are further limited by steric hindrance from neighboring residues, water molecules, and cofactors. To investigate the range of motion of the D1-Glu189 side chain within the OEC environment, we examined energy changes with respect to the dihedral angles D_2 and D_3

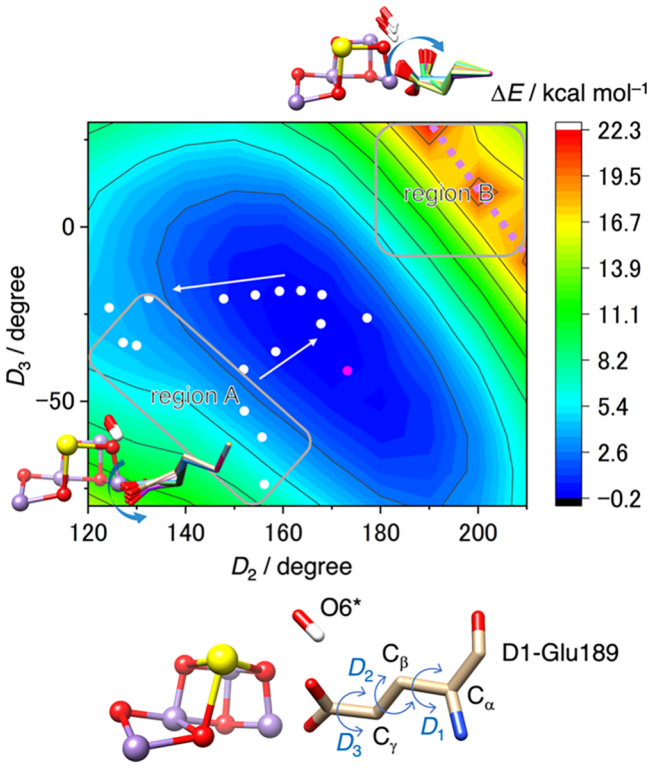

Figure 2. A potential energy surface representing the energy change (ΔE) as a function of the dihedral angles D_2 and D_3 of D1-Glu189. These calculations were based on the PDB coordinates (6JLL, monomer A),[10] with an additional O6* remaining attached to the Ca ion of the Mn cluster. The relative energy ΔE is referenced to the metastable structure depicted in Figure S1B. White circles indicate the D_2 and D_3 values corresponding to the motion of the D1-Glu189 side chain when coupled with O6* binding to Mn_D (see Figure 3). A magenta circle represents the D_2 and D_3 values observed in the S_3 state, in which O5 and O6 either form an oxyl-oxo bond or exist as bridging oxo and terminal hydroxo ligands.

using the hydrogen-bonding network (arrangement I) shown in Figure S1B. The result, presented in Figure 2, indicates that the spatial configuration of D1-Glu189 exhibits a broader range of motion than anticipated. The energy difference (ΔE), compared to a metastable structure with O6* (OH^-) bound to Ca, as depicted in Figure S1B, remains relatively low (<∼10 kcal mol^{-1}) while D_2 varies from 120° to 210° and D_3 from −80° to 30°. Notably, regions A and B in the energy landscape, as indicated in Figure 2, draw our attention, as they provide the opportunity for O6* to engage in physical interactions with Mn_D. In the region A, the carboxylate group of D1-Glu189 adopts a twisted conformation oriented toward D1-Val185, and entry into this area is achievable with an energy of around 7 kcal/mol or less. On the other hand, reaching the region B involves a twist in the carboxylate group of D1-Glu189 toward O6*. Crossing a dashed line in the energy landscape results in a substantial shift of around 20° in the D_1 dihedral angle, causing the carboxylate group to extend well beyond O6*, leaving a substantial space between O6* and Mn_D. However, this structural motion encounters an energy barrier of around 20 kcal mol^{-1} or higher, making it an impractical motion. Even with considerable space between O6* and Mn_D in the regions A and B, no spontaneous movement of O6* toward the Mn_D site was observed, as illustrated in Figure 2. This indicates that a small amount of energy is likely required to rearrange or

https://doi.org/10.1021/acsomega.4c09981
ACS Omega 2024, 9, 50041−50048

disrupt the surrounding hydrogen bonding network formed by five water molecules W10, W20, W21, W22, and W23 (arrangement I in Figure S1B), which stabilizes O6* in its anionic form (OH^-) and traps it at the Ca site.

When the Ca-bound O6* (OH^-) attempts to establish a bonding interaction with Mn_D, it faces significant hindrance due to the presence of D1-Glu189, located 3.09 Å from Ca (200 ms after 2F).[10] To gain insight into how D1-Glu189 navigates the transfer of O6* toward Mn_D, we deliberately inserted O6* into the tight space between Ca and D1-Glu189 by systematically adjusting the angle of Ca···O6*···O^--Glu189 from 60° to 160° in 10° increments. Figure 3A depicts the coordinated movements of D1-Glu189 and O6*, with their color-coding representing ΔE at each angle. The result clearly indicates that alterations in the side-chain conformation of D1-Glu189 play a guiding role, allowing O6* to enter the confined region between Ca and D1-Glu189. The dihedral angles D_2 and D_3 of the side chain shift, as illustrated by white circles in Figure 2, moving toward the region A along the most gradual slope of the potential surface when the motion of O6* is not coordinated. The energy reaches its maximum ($\Delta E \sim 13$ kcal mol^{-1}) at around an angle of 140° and a Ca···O^--Glu189 distance of 4.81 Å, beyond which O6* spontaneously binds to Mn_D. The substantial conformational change of D1-Glu189 (approaching the region A in Figure 2) is essential, though not exaggerated, for enabling O6* to move. This is more clearly understood when Ca and O^--Glu189 oxygen atoms are represented as spheres, as in Figure 3C,D. Without a conformational change in D1-Glu189, there would be significant interference between D1-Glu189 and the moving O6*, as seen in Figure 3D. However, the extensive motion of D1-Glu189 creates a narrow passage that minimally allows O6* to pass through, as depicted in Figure 3C. As O6* moves, the position of Ca fluctuates, exhibiting a maximum displacement of 0.7 Å, consistent with the experimental observation of a single negative difference density attributed to Ca disorder at time points 30 μs to 5 ms after 2F.[15] The Mn_D-bound O6*, now referred to as O6, serves not only as a hydrogen bond donor to D1-Glu189, but also continues to act as a hydrogen bond acceptor for W21 (following the water numbering in ref 15), which has been pulled into a close proximity to O6 by the movement of O6*, as indicated in Figure 3E. The presence of W21 in this position hinders D1-Glu189 from returning to its original configuration. By manually disconnecting the hydrogen bond between W21 and O6 and restoring W21 to its original position, along with altering the hydrogen-bonding pattern from arrangement I (Figure S1B) to II (Figure S1C), we confirmed that D1-Glu189 can revert to its original conformation and energetically cluster around the observed configuration (in magenta), as demonstrated in Figure 3B. We believe that such a hydrogen-bonding reorganization is likely to occur easily at room temperature. The return motion of D1-Glu189 (escaping from the region A) appears to descend a steep slope on the potential energy surface when O6* is uncoordinated (Figure 2).

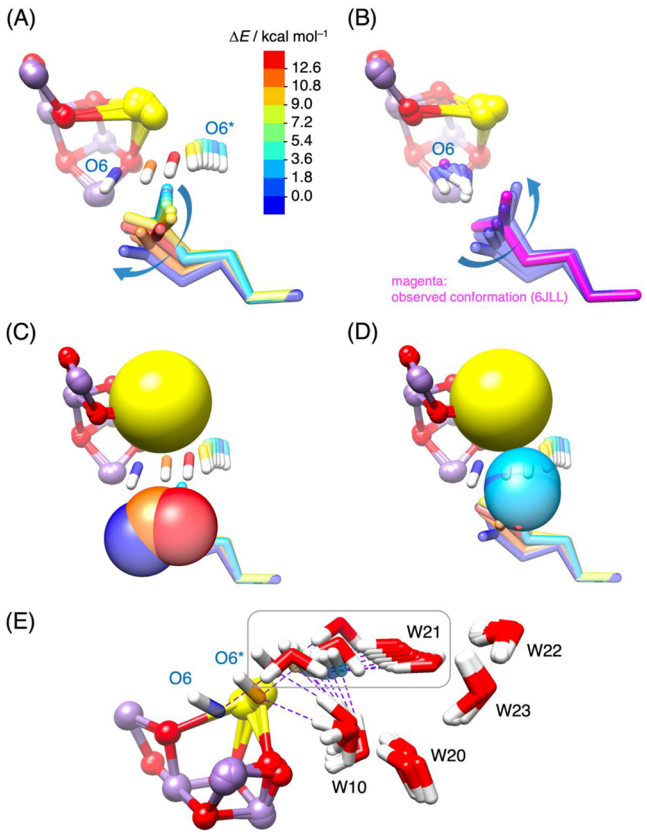

Figure 3. (A) Conformational changes in the side chain of D1-Glu189 as O6* moves toward Mn_D. The colors of O6* and D1-Glu189 correspond to the relative energy (ΔE) compared to the metastable structure shown in Figure S1B. (B) Conformational changes in the side chain of D1-Glu189 as O6* (renamed O6) binds to Mn_D, followed by the return of D1-Glu189 to its original orientation. The experimentally observed conformation in the S_3 state (6JLL, monomer A)[10] is highlighted in magenta. (C, D) A sphere representation illustrates Ca and the coordinating oxygen atoms of D1-Glu189 during O6* binding to Mn_D, aiding in the comprehension of the steric hindrance resulting from repulsive forces between neighboring Ca, D1-Glu189, and moving O6*. (E) Fluctuations of five water molecules (W10, W20, W21, W22, and W23) accompanying the movement of O6* toward Mn_D. Purple dashed lines represent hydrogen bonds between O6* and W21, as well as between O6* and W10, contributing to the stabilization of the anionic form of O6* (OH^-). As O6* moves closer to Mn_D, W21 is also pulled toward the space between Ca and D1-Glu189 due to its interaction with O6*, while interference from D1-Glu189 (not shown) causes the hydrogen bond between O6* and W10 to break just before O6* binds to Mn_D (O6* → O6).

The intricate dynamics highlighted here emphasize the pivotal role of the conformational flexibility of D1-Glu189 in facilitating the movement of O6* and its functional importance in accessing to the S_3 state with the hydroxo−oxo form (S_{total} = 3) at room temperature.[32] However, this mechanism alone does not account for the formation of the oxyl−oxo form (EPR silent, S_{total} = 6),[33−36] which is expected to emerge around 200 μs after 2F and become predominant in the low-temperature S_3 state.[10] One explanation for the discrepancy with the EPR results is the hypothesis that a reversible proton transfer may occur between O6 (OH^-) bound to Mn_D and the carboxylate oxygen of D1-Glu189, which is positioned within hydrogen bonding distance. However, previous computational studies found no evidence to support such a proton transfer.[37−39] To further investigate, we compared the relative stabilities of three chemical species in the S_3 state: hydroxo−oxo, oxyl−oxo, and deprotonated hydroxo−oxo (i.e., oxo−oxo with protonated D1-Glu189), as illustrated in Figure S2. Our analysis revealed that the hydroxo−oxo and oxyl−oxo species are nearly equally stable, which is consistent with the EPR observation that two species (S_{total} = 3 and EPR silent) could coexist or interconvert

https://doi.org/10.1021/acsomega.4c09981
ACS Omega 2024, 9, 50041−50048

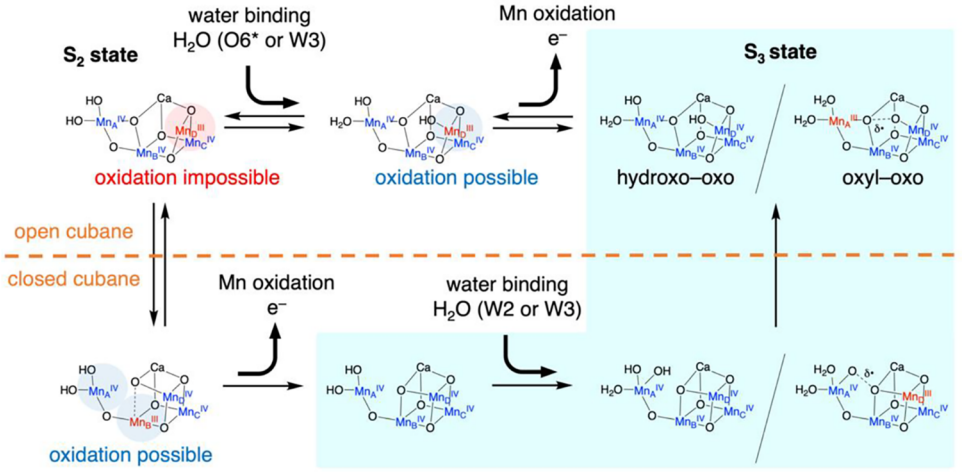

Figure 4. A proposed reaction mechanism for the S_2 to S_3 transition, based on the high-valent scheme.

under physiological conditions.[33] In contrast, the deprotonation of the hydroxo ligand to form the deprotonated hydroxo−oxo (oxo−oxo) with protonated D1-Glu189 was found to be energetically unfavorable, with an uphill energy cost exceeding 14 kcal mol^{-1} (Figure S2A), in agreement with the previous studies.[38,39] This remains true even when considering potential changes in the dihedral angles (D_1, D_2, and D_3) of the D1-Glu189 side chain (Figure S2B,C). Therefore, it is highly unlikely that D1-Glu189 is involved in storing the proton from O6 (OH^-) or mediating its release into the bulk.

Many research groups have undertaken theoretical investigations to elucidate the sequence of water molecule binding and Mn oxidation during the S_2 to S_3 transition.[40−48] The proposed sequences derived from the high-valent scheme,[49,50] in which the Mn oxidation state in the S_2 state is $Mn_A^{IV}Mn_B^{IV}Mn_C^{IV}Mn_D^{III}$, intricately intertwine with the structural rearrangements of the Mn cluster. The basis for this deduction lies in the fact that a five-coordinated Mn_D^{III} cannot undergo oxidation unless one of the three amino acid ligands (D1-Glu189, D1-Asp342, and D1-His332) is replaced by a water-derived ligand. This conclusion remains robust, with no successful instances of realizing a five-coordinated Mn_D^{IV} in any theoretical investigations. Building upon this computational evidence grounded in the high-valent scheme, we recently proposed a reaction scheme outlined in Figure 4.[44,45] If there are no significant changes in the framework of the Mn cluster, known as the open cubane structure, the sequence comprises water binding as the initial step, followed by Mn oxidation, as demonstrated by the order indicated above the dashed line in Figure 4. While it has been conventionally assumed that the bound water originates from W3 or W2, the latest XFEL study suggests a novel possibility that O6* could serve as the direct source of the bound water.[15] This proposition holds significant implications if O6* indeed represents an OH^- ion, as illustrated in Figure 3. However, current knowledge does not entirely rule out the possibility that O6* might actually be H_2O. The uncertainty surrounding this issue stems from the inherent characteristics of Ca^{2+}, which typically exhibit relatively low Lewis acidity compared to Mn. In this scenario, the specificity of O6* may be diminished. As W2, W3, and O6* are all water molecules (H_2O), it becomes unclear which one is responsible for the Mn_D-bound O6. The ambiguity arises because, in all cases, they produce the same final products, making it difficult to distinguish their individual contributions to the reaction. The propensity of Ca^{2+} and O6* (H_2O) to dissociate at the current level of theory (B3LYP/BS1) further complicates the assessment of whether O6* (H_2O) serves as the substrate for the ongoing cycle or the subsequent one. Therefore, the ambiguous nature of O6* (whether it is OH^- or H_2O) adds a layer of complexity to the mechanistic understanding of the S_2−S_3 transition, intertwined with the sequence of water binding and Mn oxidation, as well as the structural rearrangement of the Mn cluster. Considering the ligand-exchange activity of Mn^{III} and the ligand-exchange inertness of Mn^{IV}, it is reasonable to suggest that the attachment of O6* to Mn_D^{III} may be reversible. This opens up the possibility for an alternative mechanistic pathway where Mn oxidation precedes water binding to the Mn^{IV} site. Such a pathway would require the transient formation of a closed cubane structure,[51−53] as exemplified by the sequence indicated below the dashed line in Figure 4. This dual-pathway model suggests a level of mechanistic flexibility that enables the OEC to adapt to varying physiological conditions. The reversibility for O6* motion is in line with the persistent presence of residual density for O6*, which remains detectable even in the S_3 state (at a time point of 5 ms after 2F),[15] as well as membrane-inlet mass spectrometry (MIMS) measurements, which detected substrate water $^{16}O/^{18}O$ exchange after the incubation of the PSII in the S_3 state in the presence of $H_2{}^{18}O$.[54−56]

In these contexts, future research should adopt a broader perspective that explores the distinct structural characteristics extending beyond the immediate coordination spheres, while also assessing how these features interact with physiological conditions such as pH, temperature, and the presence of cryoprotectants or other environmental additives. The catalytic environment of the OEC differs across organisms like cyanobacteria and higher plants due to differences in protein composition, secondary ligand environments, and cofactors. These differences, combined with environmental factors, may influence the efficiency and mechanistic pathways involved in the uptake and binding of water molecules to the OEC.[33,57−65] A comprehensive approach that considers these aspects may provide valuable insights into how nature optimizes water uptake and coordination, as well as associated processes such as electron transfer and proton transport, across different species and environmental contexts, ultimately advancing our understanding of biological water oxidation.

https://doi.org/10.1021/acsomega.4c09981
ACS Omega 2024, 9, 50041−50048

4. CONCLUSIONS

In this study, we focused on elucidating the specific role of the D1-Glu189 amino acid residue within the OEC to better understand how the conformational flexibility of its side chain influences the selective attraction, guidance, and stabilization of a substrate water molecule. This study is based on the currently tested hypothesis that during the S_2 to S_3 transition, a specific water molecule (O6*) may transiently associate with a Ca ion, stabilizing as a hydroxide ion (OH^-).[15] Our detailed analysis demonstrates a critical mechanism in the catalytic function of the OEC, specifically highlighting the detachment of the D1-Glu189 carboxylate group from its coordination with the Ca ion. This detachment triggers a significant reorganization of the local protein environment, resulting in the formation of a transient but well-defined binding passage within the OEC. This passage serves as a selective gateway, effectively attracting O6* in its deprotonated form from the surrounding pool of water molecules and directing its transition from a loosely coordinated state at the Ca ion to a more stable, catalytically active position at the Mn_D site. Once at this site, O6* undergoes further structural adjustments, acquiring the necessary chemical properties to act as a substrate water molecule, now referred to as O6. This optimal positioning of O6 at the catalytic center is crucial for enabling the series of subsequent oxidation steps required for the progression of the water-splitting catalytic cycle. These findings suggest that the conformational flexibility of D1-Glu189 is not merely a passive characteristic but could actively contribute to shaping the specialized microenvironment within the OEC and supporting key catalytic processes.

■ ASSOCIATED CONTENT

Supporting Information

The Supporting Information is available free of charge at https://pubs.acs.org/doi/10.1021/acsomega.4c09981.

Overall view of the OEC model; energetics for proton transfer between O6 and D1-Glu189; and Cartesian coordinates for two selected structures in Figure 3A (PDF)

■ AUTHOR INFORMATION

Corresponding Author

Hiroshi Isobe − *Research Institute for Interdisciplinary Science, Okayama University, Okayama 700-8530, Japan;* orcid.org/0000-0002-1990-1904; Email: h-isobe@cc.okayama-u.ac.jp

Authors

Takayoshi Suzuki − *Research Institute for Interdisciplinary Science, Okayama University, Okayama 700-8530, Japan;* orcid.org/0000-0002-6886-242X

Michihiro Suga − *Research Institute for Interdisciplinary Science, Okayama University, Okayama 700-8530, Japan*

Jian-Ren Shen − *Research Institute for Interdisciplinary Science, Okayama University, Okayama 700-8530, Japan;* orcid.org/0000-0003-4471-8797

Kizashi Yamaguchi − *Center for Quantum Information and Quantum Biology, Osaka University, Toyonaka, Osaka 560-0043, Japan*

Complete contact information is available at: https://pubs.acs.org/10.1021/acsomega.4c09981

Notes

The authors declare no competing financial interest.

■ ACKNOWLEDGMENTS

This work was supported by JSPS KAKENHI Grant Number JP22K05317. The computation was performed using Research Center for Computational Science, Okazaki, Japan.

■ REFERENCES

(1) *Photosystem II: The Light Driven Water: Plastoquinone Oxidoreductase*; Wydrzynski, T. J.; Satoh, K., Eds.; Springer: Dordrecht, The Netherlands, 2005.

(2) Barber, J.; Tran, P. D. From natural to artificial photosynthesis. *J. R. Soc., Interface* **2013**, *10*, 20120984.

(3) Blakemore, J. D.; Crabtree, R. H.; Brudvig, G. W. Molecular catalysts for water oxidation. *Chem. Rev.* **2015**, *115*, 12974−13005.

(4) McEvoy, J. P.; Brudvig, G. W. Water-splitting chemistry of photosystem II. *Chem. Rev.* **2006**, *106*, 4455−4483.

(5) Cox, N.; Pantazis, D. A.; Neese, F.; Lubitz, W. Biological water oxidation. *Acc. Chem. Res.* **2013**, *46*, 1588−1596.

(6) Yano, J.; Yachandra, V. K. Mn_4Ca cluster in photosynthesis: where and how water is oxidized to dioxygen. *Chem. Rev.* **2014**, *114*, 4175−4205.

(7) Shen, J.-R. The structure of photosystem II and the mechanism of water oxidation in photosynthesis. *Annu. Rev. Plant Biol.* **2015**, *66*, 23−48.

(8) Suga, M.; Akita, F.; Sugahara, M.; Kubo, M.; Nakajima, Y.; Nakane, T.; Yamashita, K.; Umena, Y.; Nakabayashi, M.; Yamane, T.; Nakano, T.; Suzuki, M.; Masuda, T.; Inoue, S.; Kimura, T.; Nomura, T.; Yonekura, S.; Yu, L.-J.; Sakamoto, T.; Motomura, T.; Chen, J.-H.; Kato, Y.; Noguchi, T.; Tono, K.; Joti, Y.; Kameshima, T.; Hatsui, T.; Nango, E.; Tanaka, R.; Naitow, H.; Matsuura, Y.; Yamashita, A.; Yamamoto, M.; Nureki, O.; Yabashi, M.; Ishikawa, T.; Iwata, S.; Shen, J.-R. Light-induced structural changes and the site of O = O bond formation in PSII caught by XFEL. *Nature* **2017**, *543*, 131−135.

(9) Kern, J.; Chatterjee, R.; Young, I. D.; Fuller, F. D.; Lassalle, L.; Ibrahim, M.; Gul, S.; Fransson, T.; Brewster, A. S.; Alonso-Mori, R.; Hussein, R.; Zhang, M.; Douthit, L.; de Lichtenberg, C.; Cheah, M. H.; Shevela, D.; Wersig, J.; Seuffert, I.; Sokaras, D.; Pastor, E.; Weninger, C.; Kroll, T.; Sierra, R. G.; Aller, P.; Butryn, A.; Orville, A. M.; Liang, M.; Batyuk, A.; Koglin, J. E.; Carbajo, S.; Boutet, S.; Moriarty, N. W.; Holton, J. M.; Dobbek, H.; Adams, P. D.; Bergmann, U.; Sauter, N. K.; Zouni, A.; Messinger, J.; Yano, J.; Yachandra, V. K. Structures of the intermediates of Kok's photosynthetic water oxidation clock. *Nature* **2018**, *563*, 421−425.

(10) Suga, M.; Akita, F.; Yamashita, K.; Nakajima, Y.; Ueno, G.; Li, H.; Yamane, T.; Hirata, K.; Umena, Y.; Yonekura, S.; Yu, L.-J.; Murakami, H.; Nomura, T.; Kimura, T.; Kubo, M.; Baba, S.; Kumasaka, T.; Tono, K.; Yabashi, M.; Isobe, H.; Yamaguchi, K.; Yamamoto, M.; Ago, H.; Shen, J.-R. An oxyl/oxo mechanism for oxygen-oxygen coupling in PSII revealed by an x-ray free-electron laser. *Science* **2019**, *366*, 334−338.

(11) Ibrahim, M.; Fransson, T.; Chatterjee, R.; Cheah, M. H.; Hussein, R.; Lassalle, L.; Sutherlin, K. D.; Young, I. D.; Fuller, F. D.; Gul, S.; Kim, I.-S.; Simon, P. S.; de Lichtenberg, C.; Chernev, P.; Bogacz, I.; Pham, C. C.; Orville, A. M.; Saichek, N.; Northen, T.; Batyuk, A.; Carbajo, S.; Alonso-Mori, R.; Tono, K.; Owada, S.; Bhowmick, A.; Bolotovsky, R.; Mendez, D.; Moriarty, N. W.; Holton, J. M.; Dobbek, H.; Brewster, A. S.; Adams, P. D.; Sauter, N. K.; Bergmann, U.; Zouni, A.; Messinger, J.; Kern, J.; Yachandra, V. K.; Yano, J. Untangling the sequence of events during the S2 → S3 transition in photosystem II and implications for the water oxidation mechanism. *Proc. Natl. Acad. Sci. U.S.A.* **2020**, *117*, 12624−12635.

(12) Hussein, R.; Ibrahim, M.; Bhowmick, A.; Simon, P. S.; Chatterjee, R.; Lassalle, L.; Doyle, M.; Bogacz, I.; Kim, I.-S.; Cheah, M. H.; Gul, S.; de Lichtenberg, C.; Chernev, P.; Pham, C. C.; Young, I. D.; Carbajo, S.; Fuller, F. D.; Alonso-Mori, R.; Batyuk, A.; Sutherlin, K. D.; Brewster, A. S.; Bolotovsky, R.; Mendez, D.; Holton, J. M.;

Moriarty, N. W.; Adams, P. D.; Bergmann, U.; Sauter, N. K.; Dobbek, H.; Messinger, J.; Zouni, A.; Kern, J.; Yachandra, V. K.; Yano, J. Structural dynamics in the water and proton channels of photosystem II during the S_2 to S_3 transition. *Nat. Commun.* **2021**, *12*, 6531.
(13) Li, H.; Nakajima, Y.; Nomura, T.; Sugahara, M.; Yonekura, S.; Chan, S. K.; Nakane, T.; Yamane, T.; Umena, Y.; Suzuki, M.; Matsuda, T.; Motomura, T.; Naitow, H.; Matsuura, Y.; Kimura, T.; Tono, K.; Owada, S.; Joti, Y.; Tanaka, R.; Nango, E.; Akita, F.; Kubo, M.; Iwata, S.; Shen, J.-R.; Suga, M. Capturing structural changes of the S_1 to S_2 transition of photosystem II using time-resolved serial femtosecond crystallography. *IUCrJ.* **2021**, *8*, 431−443.
(14) Bhowmick, A.; Hussein, R.; Bogacz, I.; Simon, P. S.; Ibrahim, M.; Chatterjee, R.; Doyle, M. D.; Cheah, M. H.; Fransson, T.; Chernev, P.; Kim, I.-S.; Makita, H.; Dasgupta, M.; Kaminsky, C. J.; Zhang, M.; Gätcke, J.; Haupt, S.; Nangca, I. I.; Keable, S. M.; Aydin, A. O.; Tono, K.; Owada, S.; Gee, L. B.; Fuller, F. D.; Batyuk, A.; Alonso-Mori, R.; Holton, J. M.; Paley, D. W.; Moriarty, N. W.; Mamedov, F.; Adams, P. D.; Brewster, A. S.; Dobbek, H.; Sauter, N. K.; Bergmann, U.; Zouni, A.; Messinger, J.; Kern, J.; Yano, J.; Yachandra, V. K. Structural evidence for intermediates during O_2 formation in photosystem II. *Nature* **2023**, *617*, 629−636.
(15) Li, H.; Nakajima, Y.; Nango, E.; Owada, S.; Yamada, D.; Hashimoto, K.; Luo, F.; Tanaka, R.; Akita, F.; Kato, K.; Kang, J.; Saitoh, Y.; Kishi, S.; Yu, H.; Matsubara, N.; Fujii, H.; Sugahara, M.; Suzuki, M.; Masuda, T.; Kimura, T.; Thao, T. N.; Yonekura, S.; Yu, L.-J.; Tosha, T.; Tono, K.; Joti, Y.; Hatsui, T.; Yabashi, M.; Kubo, M.; Iwata, S.; Isobe, H.; Yamaguchi, K.; Suga, M.; Shen, J.-R. Oxygen-evolving photosystem II structures during S_1−S_2−S_3 transitions. *Nature* **2024**, *626*, 670−677.
(16) Umena, Y.; Kawakami, K.; Shen, J.-R.; Kamiya, N. Crystal structure of oxygen-evolving photosystem II at a resolution of 1.9 Å. *Nature* **2011**, *473*, 55−60.
(17) Tanaka, A.; Fukushima, Y.; Kamiya, N. Two different structures oft he oxygen-evolving complex in the same polypeptide frameworks of photosystem II. *J. Am. Chem. Soc.* **2017**, *139*, 1718−1721.
(18) Suga, M.; Akita, F.; Hirata, K.; Ueno, G.; Murakami, H.; Nakajima, Y.; Shimizu, T.; Yamashita, K.; Yamamoto, M.; Ago, H.; Shen, J.-R. Native structure of photosystem II at 1.95 Å resolution viewed by femtosecond X-ray pulses. *Nature* **2015**, *517*, 99−103.
(19) Becke, A. D. Density-functional exchange-energy approximation with correct asymptotic behavior. *Phys. Rev. A* **1988**, *38*, 3098−3100.
(20) Lee, C.; Yang, W.; Parr, R. G. Development of the Colle-Salvetti correction-energy formula into a functional of the electron density. *Phys. Rev. B* **1988**, *37*, 785−789.
(21) Becke, A. D. Density-functional thermochemistry. III. The role of exact exchange. *J. Chem. Phys.* **1993**, *98*, 5648−5652.
(22) Grimme, S.; Antony, J.; Ehrlich, S.; Krieg, H. A Consistent and accurate Ab Initio parameterization of density functional dispersion correction (DFT-D) for the 94 elements H-Pu. *J. Chem. Phys.* **2010**, *132*, 154104.
(23) Grimme, S.; Ehrlich, S.; Goerigk, L. Effects of the damping function in dispersion corrected density functional theory. *J. Comput. Chem.* **2011**, *32*, 1456−1465.
(24) Frisch, M. J.; Trucks, G. W.; Schlegel, H. B.; Scuseria, G. E.; Robb, M. A.; Cheeseman, J. R.; Scalmani, G.; Barone, V.; Petersson, G. A.; Nakatsuji, H.; Li, X.; Caricato, M.; Marenich, A. V.; Bloino, J.; Janesko, B. G.; Gomperts, R.; Mennucci, B.; Hratchian, H. P.; Ortiz, J. V.; Izmaylov, A. F.; Sonnenberg, J. L.; Williams-Young, D.; Ding, F.; Lipparini, F.; Egidi, F.; Goings, J.; Peng, B.; Petrone, A.; Henderson, T.; Ranasinghe, D.; Zakrzewski, V. G.; Gao, J.; Rega, N.; Zheng, G.; Liang, W.; Hada, M.; Ehara, M.; Toyota, K.; Fukuda, R.; Hasegawa, J.; Ishida, M.; Nakajima, T.; Honda, Y.; Kitao, O.; Nakai, H.; Vreven, T.; Throssell, K.; Montgomery, J. A., Jr.; Peralta, J. E.; Ogliaro, F.; Bearpark, M. J.; Heyd, J. J.; Brothers, E. N.; Kudin, K. N.; Staroverov, V. N.; Keith, T. A.; Kobayashi, R.; Normand, J.; Raghavachari, K.; Rendell, A. P.; Burant, J. C.; Iyengar, S. S.; Tomasi, J.; Cossi, M.; Millam, J. M.; Klene, M.; Adamo, C.; Cammi, R.; Ochterski, J. W.; Martin, R. L.; Morokuma, K.; Farkas, O.; Foresman, J. B.; Fox, D. J. *Gaussian 16, Revision C.01*; Gaussian, Inc.: Wallingford, CT, 2016.
(25) Hay, P. J.; Wadt, W. R. Ab initio effective core potentials for molecular calculations. Potentials for the transition metal atoms Sc to Hg. *J. Chem. Phys.* **1985**, *82*, 270−283.
(26) Wadt, W. R.; Hay, P. J. Ab initio effective core potentials for molecular calculations. Potentials for main group elements Na to Bi. *J. Chem. Phys.* **1985**, *82*, 284−298.
(27) Hay, P. J.; Wadt, W. R. Ab initio effective core potentials for molecular calculations. Potentials for K to Au including the outermost core orbitals. *J. Chem. Phys.* **1985**, *82*, 299−310.
(28) Reiher, M.; Salomon, O.; Hess, B. A. Reparameterization of hybrid functionals based on energy differences of states of different multiplicity. *Theor. Chem. Acc.* **2001**, *107*, 48−55.
(29) Dolg, M.; Wedig, U.; Stoll, H.; Preuss, H. Energy-adjusted ab initio pseudopotentials for the first row transition elements. *J. Chem. Phys.* **1987**, *86*, 866−872.
(30) Kaupp, M.; Schleyer, P. v. R.; Stoll, H.; Preuss, H. Pseudopotential approaches to Ca, Sr, and Ba hydrides. Why are some alkaline earth MX_2 compounds bent? *J. Chem. Phys.* **1991**, *94*, 1360−1366.
(31) Tomasi, J.; Mennucci, B.; Cammi, R. Quantum mechanical continuum solvation models. *Chem. Rev.* **2005**, *105*, 2999−3093.
(32) Cox, N.; Retegan, M.; Neese, F.; Pantazis, D. A.; Boussac, A.; Lubitz, W. Electronic structure of the oxygen-evolving complex in photosystem II prior to O−O bond formation. *Science* **2014**, *345*, 804−808.
(33) Boussac, A.; Rutherford, A. W.; Sugiura, M. Electron transfer pathways from the S_2-state to the S_3-state either after a Ca^{2+}/Sr^{2+} or Cl^-/I^- exchange in photosystem II from *Thermosynechococcus elongatus*. *Biochim. Biophys. Acta* **2015**, *1847*, 576−586.
(34) Isobe, H.; Shoji, M.; Shen, J.-R.; Yamaguchi, K. Chemical equilibrium models for the S_3 state of the oxygen-evolving complex of photosystem II. *Inorg. Chem.* **2016**, *55*, 502−511.
(35) Isobe, H.; Shoji, M.; Suzuki, T.; Shen, J.-R.; Yamaguchi, K. Spin, valence, and structural isomerism in the S_3 state of the oxygen-evolving complex of photosystem II as a manifestation of multi-metallic cooperativity. *J. Chem. Theory Comput.* **2019**, *15*, 2375−2391.
(36) Rummel, F.; O'Malley, P. J. How nature makes O_2: an electronic level mechanism for water oxidation in photosynthesis. *J. Phys. Chem. B* **2022**, *126*, 8214−8221.
(37) Narzi, D.; Capone, M.; Bovi, D.; Guidoni, L. Evolution from S_3 to S_4 states of the oxygen-evolving complex in photosystem II monitored by quantum mechanics/molecular mechanics (QM/MM) dynamics. *Chem. − Eur. J.* **2018**, *24*, 10820−10828.
(38) Mandal, M.; Saito, K.; Ishikita, H. The nature of the short oxygen−oxygen distance in the Mn_4CaO_6 complex of photosystem II crystals. *J. Phys. Chem. Lett.* **2020**, *11*, 10262−10268.
(39) Malcomson, T.; Rummel, F.; O'Malley, P. Hey ho, where'd the proton go? Final deprotonation of O6 within the S_3 state of photosystem II. *J. Photochem. Photobiol., B* **2024**, *257*, No. 112946.
(40) Narzi, D.; Bovi, D.; Guidoni, L. Pathway for Mn-cluster oxidation by tyrosine-Z in the S_2 state of photosystem II. *Proc. Natl. Acad. Sci. U.S.A.* **2014**, *111*, 8723−8728.
(41) Retegan, M.; Krewald, V.; Mamedov, F.; Neese, F.; Lubitz, W.; Cox, N.; Pantazis, D. A. A five-coordinate Mn(IV) intermediate in biological water oxidation: spectroscopic signature and a pivot mechanism for water binding. *Chem. Sci.* **2016**, *7*, 72−84.
(42) Siegbahn, P. E. M. The S_2 to S_3 transition for water oxidation in PSII (photosystem II), revisited. *Phys. Chem. Chem. Phys.* **2018**, *20*, 22926−22931.
(43) Pushkar, Y.; Ravari, A. K.; Jensen, S. C.; Palenik, M. Early binding of substrate oxygen is responsible for a spectroscopically distinct S_2 state in photosystem II. *J. Phys. Chem. Lett.* **2019**, *10*, 5284−5291.
(44) Isobe, H.; Shoji, M.; Suzuki, T.; Shen, J.-R.; Yamaguchi, K. Exploring reaction pathways for the structural rearrangements of the Mn cluster induced by water binding in the S_3 state of the oxygen

https://doi.org/10.1021/acsomega.4c09981
ACS Omega 2024, 9, 50041−50048

evolving complex of photosystem II. *J. Photochem. Photobiol., A* **2021**, *405*, No. 112905.
(45) Isobe, H.; Shoji, M.; Suzuki, T.; Shen, J.-R.; Yamaguchi, K. Roles of the flexible primary coordination sphere of the Mn_4CaO_X cluster: what are the immediate decay products of the S_3 state? *J. Phys. Chem. B* **2022**, *126*, 7212−7228.
(46) Allgöwer, F.; Gamiz-Hernandez, A. P.; Rutherford, A. W.; Kaila, V. R. Molecular principles of redox-coupled protonation dynamics in photosystem II. *J. Am. Chem. Soc.* **2022**, *144*, 7171−7180.
(47) Guo, Y.; Messinger, J.; Kloo, L.; Sun, L. Reversible structural isomerization of nature's water oxidation catalyst prior to O−O bond formation. *J. Am. Chem. Soc.* **2022**, *144*, 11736−11747.
(48) Liu, J.; Yang, K. R.; Long, Z.; Armstrong, W. H.; Brudvig, G. W.; Batista, V. S. Water ligands regulate the redox leveling mechanism of the oxygen-evolving complex of the photosystem II. *J. Am. Chem. Soc.* **2024**, *146*, 15986−15999.
(49) Krewald, V.; Retegan, M.; Cox, N.; Messinger, J.; Lubitz, W.; DeBeer, S.; Neese, F.; Pantazis, D. A. Metal oxidation states in biological water splitting. *Chem. Sci.* **2015**, *6*, 1676−1695.
(50) Cheah, M. H.; Zhang, M.; Shevela, D.; Mamedov, F.; Zouni, A.; Messinger, J. Assessment of the manganese cluster's oxidation state via photoactivation of photosystem II microcrystals. *Proc. Natl. Acad. Sci. U.S.A.* **2020**, *117*, 141−145.
(51) Isobe, H.; Shoji, M.; Yamanaka, S.; Umena, Y.; Kawakami, K.; Kamiya, K.; Shen, J.-R.; Yamaguchi, K. Theoretical illumination of water-inserted structures of the $CaMn_4O_5$ cluster in the S_2 and S_3 states of the oxygen-evolving complex of photosystem II: full geometry optimizations by B3LYP hybrid density functional. *Dalton Trans.* **2012**, *41*, 13727−13740.
(52) Pantazis, D. A.; Ames, W.; Cox, N.; Lubitz, W.; Neese, F. Two interconvertible structures that explain the spectroscopic properties of the oxygen-evolving complex of photosystem II in the S_2 state. *Angew. Chem., Int. Ed.* **2012**, *51*, 9935−9940.
(53) Bovi, D.; Narzi, D.; Guidoni, L. The S_2 state of the oxygen-evolving complex of photosystem II explored by QM/MM dynamics: spin surfaces and metastable states suggest a reaction path towards the S_3 state. *Angew. Chem., Int. Ed.* **2013**, *52*, 11744−11749.
(54) Hillier, W.; Wydrzynski, T. Oxygen ligand exchange at metal sites−implications for the O_2 evolving mechanism of photosystem II. *Biochim. Biophys. Acta* **2001**, *1503*, 197−209.
(55) Hillier, W.; Wydrzynski, T. ^{18}O-water exchange in photosystem II: substrate binding and intermediates of the water splitting cycle. *Coord. Chem. Rev.* **2008**, *252*, 306−317.
(56) Cox, N.; Messinger, J. Reflections on substrate water and dioxygen formation. *Biochim. Biophys. Acta* **2013**, *1827*, 1020−1030.
(57) Haddy, A. EPR spectroscopy of the manganese cluster of photosystem II. *Photosynth. Res.* **2007**, *92*, 357−368.
(58) Pokhrel, R.; Brudvig, G. W. Oxygen-evolving complex of photosystem II: correlating structure with spectroscopy. *Phys. Chem. Chem. Phys.* **2014**, *16*, 11812−11821.
(59) Boussac, A.; Ugur, I.; Marion, A.; Sugiura, M.; Kaila, V. R. I.; Rutherford, A. W. The low spin−high spin equilibrium in the S_2-state of the water oxidizing enzyme. *Biochim. Biophys. Acta* **2018**, *1859*, 342−356.
(60) Boussac, A. Temperature dependence of the high-spin S_2 to S_3 transition in photosystem II. *Biochim. Biophys. Acta* **2019**, *1860*, 508−518.
(61) Zimmermann, J. L.; Rutherford, A. W. Electron paramagnetic resonance properties of the S2 state of the oxygen-evolving complex of photosystem II. *Biochemistry* **1986**, *25*, 4609−4615.
(62) Beck, W. F.; Brudvig, G. W. Binding of Amines to the O_2-evolving center of photosystem II. *Biochemistry* **1986**, *25*, 6479−6486.
(63) Boussac, A.; Rutherford, A. W.; Styring, S. Interaction of ammonia with the water splitting enzyme of photosystem II. *Biochemistry* **1990**, *29*, 24−32.
(64) Retegan, M.; Pantazis, D. A. Interaction of methanol with the oxygen-evolving complex: atomistic models, channel identification, species dependence, and mechanistic implication. *Chem. Sci.* **2016**, *7*, 6463−6476.
(65) Drosou, M.; Pantazis, D. A. Comprehensive evaluation of models for ammonia binding to the oxygen evolving complex of photosystem II. *J. Phys. Chem. B* **2024**, *128*, 1333−1349.

https://doi.org/10.1021/acsomega.4c09981
ACS Omega 2024, 9, 50041−50048